

Journal of Materials Chemistry C

Accepted Manuscript



This is an *Accepted Manuscript*, which has been through the Royal Society of Chemistry peer review process and has been accepted for publication.

Accepted Manuscripts are published online shortly after acceptance, before technical editing, formatting and proof reading. Using this free service, authors can make their results available to the community, in citable form, before we publish the edited article. We will replace this *Accepted Manuscript* with the edited and formatted *Advance Article* as soon as it is available.

You can find more information about *Accepted Manuscripts* in the [Information for Authors](#).

Please note that technical editing may introduce minor changes to the text and/or graphics, which may alter content. The journal's standard [Terms & Conditions](#) and the [Ethical guidelines](#) still apply. In no event shall the Royal Society of Chemistry be held responsible for any errors or omissions in this *Accepted Manuscript* or any consequences arising from the use of any information it contains.

Synthesis and properties of highly branched sulfonated poly(arylene ether)s with flexible alkylsulfonated side chains as proton exchange membranes

Dong Liu^a, Dan Tao^a, Jiangpeng Ni^a, Xiongzhi Xiang^a, Lei Wang^{a,b,*}, Jingyu Xi^c

^a *Shenzhen Key Laboratory of Polymer Science and Technology, College of Materials Science and Engineering, Shenzhen University, Shenzhen 518060, China*

^b *Guangdong Research Center for Interfacial Engineering of Functional Materials*

^c *Institute of Green Chemistry and Energy, Graduate School at Shenzhen, Tsinghua University, Shenzhen 518055, China*

**Corresponding author: Lei Wang, E-mail: wl@szu.edu.cn*

Abstract

Comb-shaped sulfonated poly(arylene ether)s exhibit excellent properties when applied in proton exchange membranes (PEMs). However, few investigations have reported the use of comb-shaped sulfonated polymers with highly branched backbones as PEMs. In this work, a series of highly branched sulfonated poly(arylene ether)s with flexible alkylsulfonated side chains were successfully synthesized for the first time. The branched polymers were soluble in polar organic solvents and could be cast to form tough and smooth films. The membranes exhibited good overall properties as PEMs. With an increasing degree of branching (DB) value, such properties as oxidative stability, proton conductivity and swelling ratio of the membranes were significantly improved. The membrane with the highest DB value (8%) exhibits high proton conductivity (0.33 S cm^{-1} at $80 \text{ }^\circ\text{C}$) and excellent oxidative stability (445 min) as well as acceptable mechanical properties (20.51 MPa), which indicate that this material is a good candidate PEM for evaluation in fuel cell applications.

Keywords: Branched polymer, Comb-shaped poly(arylene ether)s, Oxidative stability, Proton exchange membrane.

1. Introduction

Proton exchange membrane fuel cells (PEMFCs) have attracted particular interest as an eco-friendly and efficient energy conversion system for stationary, transportation and portable applications^{1, 2}. The PEM is a critical component in PEMFCs because it transfers protons from the anode to the cathode and provides a barrier against electrons and against fuel and oxygen cross-leaks between the electrodes. Perfluorosulfonic acid polymers such as Nafion are the most promising proton-conducting polymers from the standpoint of chemical and thermal stability as well as physical and proton-conducting properties³⁻⁵. However, the high cost, low operation temperature (≤ 80 °C), high methanol crossover, and environmental recycling uncertainties of Nafion membranes limit their widespread commercial application in PEMFCs. As an alternative PEM, sulfonated poly(arylene ether)s⁶⁻⁸ have been developed over the past ten years. The sulfonated poly(arylene ether)s were found to possess good thermal stability, appropriate mechanical strength and high proton conductivity. However, most of these materials failed in their use as PEMs because of their short lifetimes when subjected to a combination of hydrolysis and oxidative degradation. Cross-linking⁹⁻¹⁷ is an effective method of improving the oxidative stability of the membranes. However, cross-linked membranes are usually insoluble in common organic solvents and are difficult to reprocess, which hinders the development of a commercial process for PEM. Therefore, it is highly necessary to improve the durability of these membranes with excellent solubility using other methods.

Recently, a series of branched PEMs were successfully prepared¹⁸⁻²⁸. Park et al.¹⁹ prepared a series of branched sulfonated polymers containing less than 0.4% branching agent using a facile method. The resultant polymers also had a positive effect on the oxidative stability and mechanical strength. Our group introduced 1,1,1-tris(4-hydroxyphenyl) ethane^{29, 30} and 1,3,5-tris[4-(4-fluorobenzoyl)phenoxy] benzene as branching agents to synthesize two series of branched nonfluorinated polymers, and the degree of branching (DB) values were 2% and 4%, respectively. The synthesized branched nonfluorinated polymers with 4% DB value exhibited better oxidative stability and proton conductivity than those with 2% DB value. Wang et al.²³ successfully prepared partially fluorinated branched sulfonated poly(ether ether ketone)s by introducing 1,3,5-tris(4-fluorobenzoyl) benzene as the branching agent, and the highest DB value was 6.67%. The membrane prepared with the branched polymer showed better oxidative stability than those with 4% DB value reported by our group^{31, 32}. These studies have demonstrated that branched polymers with good solubility exhibit improved properties in common organic solvents and therefore show great potential as PEMs materials.

More recently, a highly branched PEM with 10% DB value has been prepared^{21, 22} in our group. This membrane exhibits considerable proton conductivity and oxidative stability. Unfortunately, the tensile strength of the membrane with 10% DB value is quite low (11.5 MPa) and cannot meet the requirements for PEMFC assembly application. The microstructure of the highly branched membrane according to DB value was investigated using SEM and AFM. From the cross-section images of the

branched membrane, it was found that a rigid network structure is formed due to the branch points with hard arms and the short chain between the branching points, which decreases the chain entanglement and thus decreases the mechanical properties of the branched membranes. Therefore, we inferred that increasing the chain entanglement of branched polymers can be an effective method of improving the mechanical properties.

Comb-shaped³³⁻³⁸ sulfonated polymers with flexible side chains have been studied as PEMs and exhibit excellent properties. The flexible side chain increases the entanglement of polymer chains, which aids the membrane in forming good mechanical properties. In this work, a series of comb-shaped sulfonated polymers with highly branched backbones for PEMs were synthesized by introducing flexible side chains on the highly branched polymer backbones. The introduction of the flexible side chains is believed to increase the chain entanglement and improve the mechanical properties. The properties of the comb-shaped sulfonated polymer with highly branched backbones, including proton conductivity, hydrolysis and oxidative stabilities, mechanical properties, ion-exchange capacity (IEC), water uptake, thermal stability and swelling ratio of the membranes, were fully investigated with increasing DB value.

2. Experimental Section

2.1 Materials

1,3,5-Triphenylbenzene, 4,4-difluorodiphenyl sulfone (DFDS), 9-fluorenone, 2,6-dimethoxyphenol, 4-fluorobenzenesulfonyl, boron tribromide (BBr₃), chloride, mercaptopropionic acid (MPA), 4,4-(hexafluoroisopropylidene)diphenol (6F-BPA), 1,4-butanediol, dimethylacetamide (DMAc), dimethyl sulfoxide (DMSO), and dichloromethane were purchased from commercial sources and used as received. Toluene was dried using sodium wire, and DMAc, DMSO, and dichloromethane were dried using 4-Å molecule sieves prior to use. Anhydrous potassium carbonate was dried at 300 °C for 24 h in a furnace before use. All other solvents and reagents were reagent grade and were used as received.

2.2 Synthesis of 1,3,5-Tris[4-(4-fluorophenylsulfonyl)phenoxy]benzene (B₃)

The B₃ was synthesized from 1,3,5-triphenylbenzene and 4-fluorobenzenesulfonyl chloride using the method reported in the literature³⁹. A white powder was obtained with an overall yield of 84.8% after purification through re-crystallization from acetic acid. The structure of B₃ was confirmed using ¹H NMR.

¹H NMR (400 MHz, CDCl₃; ppm): 8.02-8.08 (m, 12 H), 7.78-7.81 (m, 9 H), 7.22-7.30 (m, 6H). Mp: 143-144 °C.

2.3 Synthesis of 9,9-Bis(3,5-dimethoxy-4-hydroxyphenyl)fluorene (DMHF)

The DMHF was synthesized from 2,6-dimethoxyphenol and 9-fluorenone using the method reported in the literature⁴⁰. The crude product was re-crystallized from toluene twice to yield 11.44 g (yield: 60%) of pure white crystalline DMHF. The

structure of DMHF was confirmed using ^1H NMR.

^1H NMR (400 MHz, DMSO-d_6 ; ppm): 8.34 (s, 2H, -OH), 7.90 (d, 2H), 7.50 (d, 2H), 7.40 (t, 2H), 7.30 (t, 2H), 6.31 (s, 4H), 3.53 (s, 12H, $-\text{OCH}_3$). Mp: 186-187 °C.

2.4 Synthesis of Poly(arylene ether sulfone)s Containing Methoxy Groups (MPAES-x-y)

As shown in Scheme 1, the MPAES-x-y polymers [x:100 B_3 /(DMHF+6F-BPA), y:100 DMHF/(DMHF+6F-BPA)] were successfully synthesized. The polymerization procedure for MPAES-8-33, which represents a typical example for the synthesis of the polymers, is described as follows: 0.2496 g (0.32 mmol) of B_3 , 0.6024 g (1.32 mmol) of DMHF, 0.9011 g (2.68 mmol) of 6F-BPA, 0.8950 g (3.52 mmol) of 4,4'-difluorodiphenyl sulfone, 0.828 g (6 mmol) of K_2CO_3 , 10 mL of DMAc, and 10 mL of toluene were carefully introduced into a 50-mL three-neck round bottom flask equipped with a Dean-Stark trap and condenser under nitrogen protection. Toluene was used as azeotropic solvent to remove the water formed during the reaction. The reaction mixture was heated at 140 °C for 4.0 h to remove the water produced, and the temperature was subsequently increased to 170 °C (oil bath temperature) to distill the toluene. The reaction mixture was held at this temperature for 3-5 h. After cooling, the resulting viscous mixture was diluted with 5 mL of DMAc and poured slowly into a 100-mL mixture of deionized water and methanol containing 2 mL of concentrated HCl to precipitate the formed polymer. The precipitates were filtered and washed with water three times to remove inorganic salts. The fibrous polymer was collected and dried at 110 °C under vacuum for 24 h (Yield: 96 %).

^1H NMR (400 MHz, CDCl_3 ; ppm): 7.60-8.04 (m, 0.55H), 7.71-7.92 (m, 4H), 7.31-7.51 (m, 1H), 6.99-7.10 (m, 7.45H), 6.82-6.88 (m, 1H), 6.48(d, H), 3.55 (s, 3H, $-\text{OCH}_3$).

2.5 Conversion of a Methoxy Group (MPAES-xx) to a Hydroxyl Group (HPAES-x-y)

The demethylation reaction is described as follows. The MPAAEN (3 g) was dissolved into 100 mL of anhydrous dichloromethane in a 500-mL three-neck flask with a nitrogen inlet. The BBr_3 (3 mL) was mixed with CH_2Cl_2 (30 mL), and the resulting solution was added dropwise to the MPAES-8-33 solution at 0 °C (ice bath). After 6 h, the resulting polymer (HPAES-8-33) was filtered, washed with methanol and deionized water, recovered, and finally dried under vacuum at 100 °C for 24 h (yield: 94 %).

^1H NMR (400 MHz, DMSO-d_6 ; ppm): 9.75 (s, 1H, $-\text{OH}$), 8.36-8.40 (m, 0.55H), 7.27-7.94 (m, 5H), 7.51-7.68 (d, 7.45H), 7.14-7.22 (m, 1H), 6.59-6.64 (d, 1H).

2.6 Preparation of Sulfonated Polymer (SHPAES-x-y)

Amounts of 1.0 g of HPAES-8-33 and 0.30 g of NaOH were dissolved into 30 mL of DMSO at room temperature and stirred for 2 h under nitrogen atmosphere. Next, 1 mL of 1,4-butanediol sulfonate was added, and the reaction was heated to 100 °C for another 12 h. The resulting polymer was obtained by carefully pouring the solution into 300 mL of isopropanol, filtered, washing thoroughly with water, and dried under vacuum at 80 °C for 10 h (yield: 89%).

^1H NMR (400 MHz, DMSO-d_6 ; ppm): 8.08-8.10 (m, 0.55H), 7.80-8.01 (m, 5H),

7.19-7.36 (m, 7.45H), 6.88-6.96 (m, 1H), 6.36-6.66 (m, 1H), 3.73 (s, 2H), 2.30 (s, 2H), 1.68 (s, 2H), 1.40 (s, 2H).

2.7 Film Preparation

The dried sulfonated polymers were dissolved as 10 wt% solutions in DMAc by stirring at room temperature. The solutions were filtered, cast on glass slides and dried under vacuum at 60 °C for 24 h to obtain tough and smooth membranes. The resultant membranes were acidified with a 1 M H₂SO₄ solution for 24 h to exchange Na⁺ with H⁺. Finally, the membranes were immersed in deionized water overnight to eliminate excessive H₂SO₄ and held in deionized water for testing purposes.

2.8 Characterization

The ¹H NMR spectra reported in ppm were recorded using a Varian 400-Hz NMR instrument using tetramethylsilane (TMS) as the internal standard. Gel permeation chromatography (GPC) analysis was carried out with Waters HPLC 2695 instrument (tetrahydrofuran as eluent and polystyrene as standard). The thermal stability of the polymers was investigated at a heating rate of 10 °C min⁻¹ over a temperature range from 50 °C to 600 °C using a Q50 TGA instrument in a nitrogen environment with a flow of 50 mL min⁻¹. Tapping-mode atomic force microscope (AFM) images were acquired using a Dimension Icon scanning probe microscope.

The water uptake and swelling ratio of the membranes were measured as follows. The membrane was measured in deionized water at the desired temperature for 12 h. The membranes were taken out, wiped with tissue paper, and quickly measured to obtain their weight and length (or width). The weights of wet membranes (W_s) were

obtained by repeating this process at different temperatures. The weights of dry membranes (W_d) were obtained by weighing the films dried at 110 °C under vacuum for 24 h. The water uptake (WU , wt%) was calculated using the following equation:

$$WU = (W_s - W_d) / W_d \times 100 \%$$

The change in length was calculated from the equation:

$$\text{Swelling ratio (\%)} = (L_s - L_d) / L_d \times 100 \%$$

where L_s and L_d are the length of wet and dry membrane, respectively.

The ion-exchange capacity (IEC) of the membranes was determined by a classical titration method. The membranes were first converted to acid form and immersed in a 2 M sodium chloride solution for 24 h to exchange H^+ with Na^+ . Next, the exchanged H^+ within the solutions was titrated with a 0.01 M sodium hydroxide solution using phenolphthalein as an indicator. The IEC values were calculated via the following relationship:

$$IEC (meqg^{-1}) = (M_{NaOH} \times V_{NaOH}) / W_d$$

where M_{NaOH} and V_{NaOH} indicate the molar concentration and volume (mL), respectively, of the aqueous NaOH solution used in titration, and W_d (g) is the weight of dry membrane.

Proton conductivity measurements were conducted on the hydrated film using an impedance analyzer (Solartron 1260A) with an oscillating voltage of 10 mV and a frequency range from 10 MHz to 500 Hz. Prior to the measurement, the membrane was immersed in 1 M H_2SO_4 at room temperature for 24 h and washed to a pH of 7 with deionized water. After holding in deionized water over 12 h, the membrane (4

cm × 1 cm) was tightly clamped and placed in a closed container with the relative humidity of 100%. The entire container was placed in a temperature-controlled water bath during the measurement. The proton conductivity was calculated from the impedance data according to following equation:

$$\sigma = d/RS$$

where d and S are the thickness and the cross-sectional area of the specimen, respectively, and R is the membrane resistance measured by impedance analyzer.

Oxidative stability was investigated by immersing the membranes in Fenton's reagent (2 ppm FeSO₄ in 3% H₂O₂) at 80 °C. The oxidative stability of the membranes was characterized by the expended time during which the membranes started to break into pieces. The hydrolytic stability was also investigated by treating the membrane samples in boiling water for 8 days.

The hydration number (λ) indicates the number of water molecules absorbed per sulfonic acid group and is calculated by combining the water uptake and IEC data. Using the dry (W_d) and the wet (W_s) membrane weights, λ were calculated as follows:

$$\lambda = [(W_s - W_d)/18] \times 1000/(W_d \times IEC) = (WU \times 1000)/(18 \times IEC)$$

Membrane density was calculated from measurements of membrane dimensions and weight after drying at 110 °C for 24 h according to the method reported in the literature⁴¹.

The microscopic morphology of membranes was investigated using an atomic force microscope (AFM) with a Dimension Icon Scanning Probe Microscope.

3. Results and Discussion

3.1 Synthesis and Characterization of Monomers and Sulfonated Polymers

The structure of B_3 was confirmed by ^1H NMR, and the signals of B_3 were observed at 7.22-7.30 ppm, 7.78-7.81 ppm, and 8.02-8.08 ppm, respectively. The structure of DMHF was confirmed by ^1H NMR spectroscopy in $\text{DMSO}-d_6$. The -OH signal appeared at 8.34 ppm, and the signals at 3.55 ppm correspond to $-\text{OCH}_3$. The spectra of aromatic protons were observed at 6.31-7.90 ppm.

As illustrated in Scheme 1, the linear and branched comb-shaped poly(arylene ether sulfone) polymers MPAES-x-y containing methoxyl groups were successfully synthesized. The polymerization was studied by changing the amounts of B_3 from 0 mol% to 8 mol% relative to the mol% of bisphenol monomer employed (6F-BPA and DMHF). When the amount of B_3 was greater than 8 mol%, the branched polymers were easily crosslinked during polymerization and became insoluble in polar solvents. The branched polymer MPAES-8-33 was selected as an example for analysis of chemical structure by ^1H NMR spectroscopy in CDCl_3 . The ^1H NMR spectra of branched polymer MPAES-8-33 are exhibited in Fig. S1. The occurrence of the peaks at approximately 8.08 ppm and 8.10 ppm suggest that the B_3 moiety is introduced into the polymers, and the $-\text{OCH}_3$ proton signals at 3.55 ppm indicate that the DMHF moiety is introduced into the polymers.

The conversion of MPAES-x-y to HPAES-x-y polymer was conducted in CH_2Cl_2 using BBr_3 , and the resulting polymer was precipitated from CH_2Cl_2 solvent because of the polar nature of hydroxyl group. Fig. S2 shows the ^1H NMR spectra of

HPAES-8-33. After demethylation, the peaks at 3.55 ppm corresponding to the hydrogen atoms of methoxyl groups disappeared, whereas the new peaks for the protons of the hydroxyl groups were observed at approximately 9.75 ppm. This result indicates that the methoxyl groups were completely converted into hydroxyl groups.

The SPAES-x-y was obtained by reaction of 1,4-butanediol with HPAES-x-y in the presence of NaOH. The structures of SPAES-x-y were confirmed by ^1H NMR spectroscopy. The ^1H NMR spectra of SPAES-x-y is shown in Fig. S3. As expected, the -OH proton signal at 9.75 ppm disappeared, whereas the signals for the four sulfobutyl methylene groups (H_{13} , H_{14} , H_{15} , and H_{16}) appeared at lower frequencies. The ^1H NMR spectra of linear polymer SPAES-0-33 and branched polymer SPAES-8-33 are compared in Fig. S4. The occurrence of the peaks at approximately 7.94 ppm and 8.04 ppm in SPAES-8-33 confirmed that the B_3 moiety is introduced into the polymers. The polymers are soluble in polar organic solvents, i.e., NMP, DMAc, DMSO, and DMF, insoluble in H_2O and CH_3OH , and can be readily cast from DMAc solutions to form tough and smooth films.

3.2 Mechanical Properties

Mechanical properties are crucial to satisfying the requirements for PEMFC-assembly applications. The mechanical properties of the branched membranes were measured, and the results are listed in Table 2. The tensile strength of the linear membrane is better than those of the branched membranes. With increasing DB value, the tensile strength of the branched membranes decreases slowly. However, all of the comb-shaped sulfonated polymer membranes with highly

branched backbones show tensile strengths comparable with that of Nafion 117 (25.7 MPa). The schematic diagrams of the highly branched polymers (SPAES-main) and the comb-shaped sulfonated polymers with highly branched backbones (SPAES-side) are compared in Fig. 1. Compared with SPAEKS-main, the tensile strength of SPAES-side with similar DB value is significantly higher (Fig. 2). From the results, we can infer that the introduction of a flexible side chain is beneficial to increasing the chain entanglement, which leads to improved tensile strength of the branched polymers.

3.3 Thermal Properties

The thermal properties of the sulfonated polymers were investigated by TGA under nitrogen protection, and the 5% weight loss temperatures are listed in Table 1. All samples were preheated at 150 °C for 30 min in the TGA furnace to remove any moisture and solvent. The TGA curves of the polymers SPAES-x-y in the sulfonic acid form appear to have two distinct degradation steps (Fig. 3). The first degradation step observed at approximately 220-300 °C is associated with the thermal degradation of the (sulfo)butoxyl groups. The second degradation step at approximately 350 °C is likely related to the thermal decomposition of the polymer main chain. The $T_{d5\%}$ of linear and highly branched polymers is higher than 250 °C, which indicates that the thermal stability of the sulfonated polymers can meet the requirement of PEMFC.

3.4 Ion-exchange Capacity (IEC), Water uptake and Dimensional Stability

The IEC is an important parameter for evaluation of a PEM because it influences water uptake and proton conductivity. The IEC values were determined by a titration

method, and the measured IEC values of all the side-chain-type SPAES-x-y membranes were in the range of 1.66-1.71 meq g⁻¹ (Table 1). The IEC values slightly decreased with increasing DB value. The experimental IEC values are close to the theoretical values. This result further indicated that the sulfonate groups were successfully incorporated into the polymer by the sulfobutylation reaction without any side reactions.

The results of water uptake (wt%) are shown in Fig. 4. Compared with the linear membranes, the branched membranes exhibited higher water uptake. The water uptake of the branched polymer membranes increased significantly with increasing DB value and temperature. The IEC values of the sulfonated aromatic polymers generally dominate the water uptake. However, water uptake of the comb-shaped polymer membranes with branched backbones increased significantly with decreasing IEC values. We infer that these results are primarily due to the introduction of branching points. Water can filter into the hydrophobic region in the three-dimensional structure near the branching points, which might contribute to the high water uptake of the branched polymers. Compared with SPAEKS-main, the water uptake of SPAES-side with similar DB value is significantly lower (Fig. 5). It is attributed that the introduction of a flexible side chain leads to decrease of free volume of the branched polymers

Fig. 6 compares the dimensional swelling ratio of the side-chain-type SPAES-x-y membranes. With increasing DB value, the swelling ratio of the branched membranes decreases slightly. Compared with the linear membrane, the branched membranes

exhibited better dimensional stability. In general, water uptake of PEMs influences the dimensional stability, and excessive water uptake can deteriorate the dimensional stability, leading to high swelling and solubility. Nevertheless, the branched membranes exhibit special behavior, and the swelling ratio of the branched membranes decreases with increasing water uptake due to the increased branching points, which limit the movement of polymer chain in water and prevent swelling of the branched membranes.

3.5 Proton Conductivity and Microstructure

The proton conductivities of the side-chain-type SPAES-x-y membranes were measured in a temperature range of 30-80 °C at a relative humidity of 100%. The conductivity data are tabulated in Fig. 7. The proton conductivities of the linear and branched polymers are greater than 10^{-2} S cm⁻¹, which is the lowest value of practical interest for use as PEMs in fuel cells. It is obvious that the proton conductivities increase with increasing DB value and temperature. The membrane with the highest DB value shows the maximum proton conductivity (0.33 S cm⁻¹) at 80 °C. Compared with SPAEKS-main, the proton conductivity of SPAES-side with similar DB value is significantly higher at low DB, shown in Fig. 8. From the results, we can infer that the introduction of a flexible side chain is beneficial to increasing the phase separation, which leads to improved proton conductivity of the branched polymers at low DB. However, the water uptake played more important than phase separation in proton conductivity of the polymers at high DB. From Fig. 8, we can see that SPAEKS-main at 8% DB exhibits higher proton conductivity than SPAEKS-side. The proton

conductivities of the SPAES-x-y membranes were also measured at 80 °C under different relative humidity (RH) (30-95%) conditions compared to that of the Nafion 117 membrane and the results are shown in Fig. 9. It can be seen that for all the SPAES-x-y membranes, the proton conductivities increase with the increasing RH. They show higher proton conductivities ($0.132\text{-}0.251\text{ S cm}^{-1}$) than that of Nafion 117 (0.131 S cm^{-1}) at 95% RH. It is believed that proton conductivity depends heavily on the IEC values and water uptake of electrolyte membranes. However, the IEC values slightly decrease with increasing DB value. The excellent proton conductivity could be attributed primarily to the high water uptake of the electrolyte membranes. Furthermore, the membrane morphology plays an important role for proton transport in PEMs.

The phase morphologies of the membranes were also investigated using AFM (Fig. 10). The bright and dark regions in the images are assigned to the hard structure corresponding to the hydrophobic domains and the soft structure corresponding to the hydrophilic domains with sulfonic acid containing water, respectively. With similar DB values, the SPAES-side membrane exhibits better formation of phase-separated structures than that of the SPAEKS-main membrane, which indicates that the introduction of flexible alkyl-sulfonic acids side chains induces the formation of well-organized nanodomains. In the AFM images, both SPAES-0-33 and SPAES-8-33 membranes display formation of phase-separated structures in which the alkylated sulfonic acids aggregate into hydrophilic clusters. More organized phase-separated morphology in the SPAES-8-33 membrane can be observed than in

the SPAES-0-33 membrane, which indicates that the branched structure could induce the formation of well-organized nanodomains. The aggregation of sulfonic acids supported by the branched structure generates the well-developed nanochannel-liked morphology, which could improve the proton conduction at low IEC values.

As shown in Fig. 11, the linear and branched membranes exhibit Arrhenius-type temperature-dependant proton conductivity behavior. The activation energy (E_a) for proton conductivity was calculated according to the Arrhenius equation: $\sigma = A \exp(-E_a/RT)$, where σ is the proton conductivity (S cm^{-1}), R is the universal gas constant ($8.314 \text{ J mol}^{-1} \text{ K}^{-1}$), A is the pre-exponential factor, and T is the absolute temperature (K). The linear membrane exhibits a relatively low activation energy value (9.46 kJ mol^{-1}), which is similar to that of Nafion 117 (9.56 kJ mol^{-1})^{40,42}. With increasing DB value, the activation energy of the branched membranes shows an increasing trend. The activation energy value of SPAES-8-33 reaches as high as $14.22 \text{ kJ mol}^{-1}$. The results revealed that the membrane with higher activation energy values exhibited greater proton conductivity with increasing the temperature. This result is attributed to the increased absorption of water by the hydrophilic segments of the branched comb-shaped polymers with increasing DB value. When the temperature is increased, the water can improve the proton conductivity of the branched membranes.

3.6 Membrane Density and Hydration Number

The results of the density testing are listed in Table 2. The densities of the branched membranes decrease with increasing DB values, primarily due to the increase of branching points in the membranes. With increasing branching points, the free

volume of the branched polymer membranes increases, leading to a decrease in the density of the membranes. The free volume can also aid in trapping water, thus leading to the significant increase in water uptake. Hydration number (λ), or the number of water molecules per sulfonic acid group, was calculated by combining the water uptake and IEC data. The λ values of membrane can better reflect the proton conductivity⁴³. The results are presented in Table 2. The λ values of the branched membranes increased remarkably with increasing DB value, and the proton conductivity and λ values exhibited similar behavior.

3.7 Oxidation and hydrolytic stabilities

PEMs are known to undergo degradation resulting from hydroxyl or peroxy free radicals formed by the decomposition of H_2O_2 generated at the cathode under the operational conditions of fuel cells⁴⁴. Following a well-established procedure, the oxidative stability of the membranes was evaluated by measuring the elapsed time before membrane began to break after immersion in Fenton's reagent (2 ppm $FeSO_4$ in 3% H_2O_2) at 80 °C. The results are shown in Table 2. The branched comb-shaped polymer membranes exhibit superior oxidative stabilities compared with that of the linear polymer membrane. The membrane formed by the branched polymers SPAES-8-33 shows the best oxidative stability, and the elapsed time is 445 min, which is 2 times longer than that of the membrane formed by linear polymers (220 min) at same conditions.

The results of the oxidative stabilities of the SPAES-side and the SPAEKS-main membranes are shown in Fig. 12. With similar DB values, the SPAES-side membrane

exhibits better oxidative stabilities than that of the SPAEKS-main membrane reported by our group⁴⁵, which indicates that the introduction of flexible alkylsulfonic acids side chains can improve the oxidative stability. For the side chain-type polymers, the alkyl side chains might separate the polymer main chain from the sulfonic acid groups more effectively to maintain the main chain in a hydrophobic atmosphere that prevents or reduces the chance of radical attack.

The hydrolytic stability was also investigated by treating the membrane samples in boiling water for more than eight days. The membranes did not change in shape or appearance after the treatment. It can be concluded that no hydrolysis occurred during the treatment.

4. Conclusions

Highly branched sulfonated poly(arylene ether sulfone)s containing comb-shaped pendant sulfonated groups were successfully prepared by polycondensation reactions. The resulting polymers can be cast into transparent, flexible, and tough membranes. With increasing DB value, the water uptake, proton conductivity and oxidative stability of the branched membranes increased, while the swelling ratio and mechanical properties of the branched membranes decreased. Compared with the highly branched sulfonated polymer SPAES-main, the comb-shaped polymers with highly branched backbones exhibit better oxidation stability and mechanical properties. The membrane with the highest DB value (8 mol%) exhibits considerable proton conductivity (0.33 S cm^{-1} at $80 \text{ }^\circ\text{C}$) and oxidative stability (445 min) and offers good potential as PEMs.

Acknowledgements

The authors gratefully acknowledge the Natural Science Foundation of Guangdong Province (2015A030313546), Shenzhen Sci & Tech research grant (JCYJ20130329105010137, JCYJ 20150331142303052 and ZDSYS201507141105130) and Nanshan District special funds (FG2013JNYF0015A) for financial support.

References and Notes

1. H. Zhang and P. K. Shen, *Chemical Society reviews*, 2012, **41**, 2382-2394.
2. H. Xie, D. Tao, J. Ni, X. Xiang, C. Gao and L. Wang, *Journal of Membrane Science*, 2016, **497**, 55-66.
3. D. W. Shin, S. Y. Lee, C. H. Lee, K.-S. Lee, C. H. Park, J. E. McGrath, M. Zhang, R. B. Moore, M. D. Lingwood and L. A. Madsen, *Macromolecules*, 2013, **46**, 7797-7804.
4. K. A. Mauritz and R. B. Moore, *Chemical reviews*, 2004, **104**, 4535-4586.
5. C. F. Kins, E. Sengupta, A. Kaltbeitzel, M. Wagner, I. Lieberwirth, H. W. Spiess and M. R. Hansen, *Macromolecules*, 2014, **47**, 2645-2658.
6. L. Zeng, T. Zhao, L. An, G. Zhao and X. Yan, *Journal of Membrane Science*, 2015, **493**, 340-348.
7. M. Tatli, R. Selhorst and E. Fossum, *Macromolecules*, 2013, **46**, 4388-4394.
8. P. Wen, Z. Zhong, L. Li, A. Zhang, X.-D. Li and M.-H. Lee, *Journal of Materials Chemistry*, 2012, **22**, 22242-22249.
9. K. Wang, X. Zhang, X. Zhang, B. Yang, Z. Li, Q. Zhang, Z. Huang and Y. Wei, *Journal of Materials Chemistry C*, 2015, **3**, 1854-1860.

10. C.-W. Huang, F.-C. Chang, Y.-L. Chu, C.-C. Lai, T.-E. Lin, C.-Y. Zhu and S.-W. Kuo, *Journal of Materials Chemistry C*, 2015, **3**, 8142-8151.
11. F. Ding, S. Wang, M. Xiao, X. Li and Y. Meng, *Journal of power sources*, 2007, **170**, 20-27.
12. S. Wang, Y. Chen, M. Xiao and Y. Meng, *Journal of Applied Polymer Science*, 2013, **127**, 1981-1988.
13. H.-S. Dang and D. Kim, *international journal of hydrogen energy*, 2012, **37**, 19007-19016.
14. B. J. Sundell, K.-s. Lee, A. Nebipasagil, A. Shaver, J. R. Cook, E.-S. Jang, B. D. Freeman and J. E. McGrath, *Industrial & Engineering Chemistry Research*, 2014, **53**, 2583-2593.
15. R. Narducci, M. Di Vona and P. Knauth, *Journal of Membrane Science*, 2014, **465**, 185-192.
16. K. Si, R. Wycisk, D. Dong, K. Cooper, M. Rodgers, P. Brooker, D. Slattery and M. Litt, *Macromolecules*, 2012, **46**, 422-433.
17. H. Xie, D. Tao, X. Xiang, Y. Ou, X. Bai and L. Wang, *Journal of Membrane Science*, 2015, **473**, 226-236.
18. P. Calandra, V. T. Liveri, A. M. Ruggirello, M. Licciardi, D. Lombardo and A. Mandanici, *Journal of Materials Chemistry C*, 2015, **3**, 3198-3210.
19. L. Wang, K. Li, G. Zhu and J. Li, *Journal of Membrane Science*, 2011, **379**, 440-448.
20. P. Calandra, V. T. Liveri, A. M. Ruggirello, M. Licciardi, D. Lombardo and A.

- Mandanici, *Journal of Materials Chemistry C*, 2015, **3**, 3198-3210.
21. J. Pang, H. Zhang, X. Li, L. Wang, B. Liu and Z. Jiang, *Journal of Membrane Science*, 2008, **318**, 271-279.
22. H. Xie, D. Wang, D. Tao and L. Wang, *Journal of Power Sources*, 2014, **262**, 328-337.
23. Y. Li, M. Xie, X. Wang, D. Chao, X. Liu and C. Wang, *International Journal of Hydrogen Energy*, 2013, **38**, 12051-12059.
24. D. W. Seo, H. S. Park, S. W. Choi, Y. G. Jeong, T. W. Hong and W.-G. Kim, *Polymer journal*, 2008, **40**, 979-985.
25. K. Matsumoto, T. Higashihara and M. Ueda, *Macromolecules*, 2008, **41**, 7560-7565.
26. A. R. Hlil, S. Matsumura and A. S. Hay, *Macromolecules*, 2008, **41**, 1912-1914.
27. T. Kim, Y.-W. Choi, C.-S. Kim, T.-H. Yang and M.-N. Kim, *Journal of Materials Chemistry*, 2011, **21**, 7612-7621.
28. S. Matsumura, A. R. Hlil, C. Lepiller, J. Gaudet, D. Guay and A. S. Hay, *Macromolecules*, 2008, **41**, 277-280.
29. S. D. Mikhailenko, K. Wang, S. Kaliaguine, P. Xing, G. P. Robertson and M. D. Guiver, *Journal of Membrane Science*, 2004, **233**, 93-99.
30. S. U. D. Mikhailenko, K. P. Wang, S. Kaliaguine, P. X. Xing, G. P. Robertson and M. D. Guiver, *J Membrane Sci*, 2004, **233**, 93-99.
31. L. Wang, Z. Yang, S. Wang, S. Wang and J. Liu, *Afr. J. Microbiol. Res*, 2011, **5**, 5854-5862.

32. L. Wang, Z. W. Yang, S. C. Wang, S. Q. Wang and J. X. Liu, *Afr J Microbiol Res*, 2011, **5**, 5854-5862.
33. O. Sato, T. Kasai, M. Sato, K. Sakajiri, Y. Tsujii, S. Kang, J. Watanabe and M. Tokita, *Journal of Materials Chemistry C*, 2013, **1**, 7992-7995.
34. C. Wang, S. Y. Lee, D. W. Shin, N. R. Kang, Y. M. Lee and M. D. Guiver, *Journal of Membrane Science*, 2013, **427**, 443-450.
35. Y. Zhang, Y. Wan, C. Zhao, K. Shao, G. Zhang, H. Li, H. Lin and H. Na, *Polymer*, 2009, **50**, 4471-4478.
36. D. S. Kim, G. P. Robertson and M. D. Guiver, *Macromolecules*, 2008, **41**, 2126-2134.
37. R. Patel, S. J. Im, Y. T. Ko, J. H. Kim and B. R. Min, *Journal of Industrial and Engineering Chemistry*, 2009, **15**, 299-303.
38. J. Pang, H. Zhang, X. Li, B. Liu and Z. Jiang, *Journal of Power Sources*, 2008, **184**, 1-8.
39. X. Zhang, L. Sheng, T. Higashihara and M. Ueda, *Polym Chem-Uk*, 2013, **4**, 1235-1242.
40. C. Wang, N. Li, D. W. Shin, S. Y. Lee, N. R. Kang, Y. M. Lee and M. D. Guiver, *Macromolecules*, 2011, **44**, 7296-7306.
41. D. S. Kim, Y. S. Kim, M. D. Guiver and B. S. Pivovar, *Journal of Membrane Science*, 2008, **321**, 199-208.
42. J. Y. Chu, A. R. Kim, K. S. Nahm, H.-K. Lee and D. J. Yoo, *International Journal of Hydrogen Energy*, 2013, **38**, 6268-6274.

43. L. Sheng, T. Higashihara, M. Ueda and T. Hayakawa, *Journal of Polymer Science Part A: Polymer Chemistry*, 2014, **52**, 21-29.
44. H. Zhang and P. K. Shen, *Chemical reviews*, 2012, **112**, 2780-2832.
45. L. Wang, D. Wang, G. Zhu and J. Li, *European Polymer Journal*, 2011, **47**, 1985-1993.

Captions

Table 1. Properties of linear and branched comb-shaped polymers

Table 2. Properties of linear and branched comb-shaped membranes

Scheme 1. Synthesis of highly branched polymers MPAES-33, HPAES-33,
SPAES-33

Fig. 1 Diagrams of the linear and branched comb-shaped polymers

Fig. 2 Tensile strength of SPAEKS-main and SPAES-side

Fig. 3 TGA curves of the linear and branched comb-shaped polymers

Fig. 4 Water uptake of the linear and branched comb-shaped polymer membranes

Fig. 5 Water uptake of SPAEKS-main and SPAES-side

Fig. 6 Swelling rate of the linear and branched comb-shaped polymer membranes

Fig. 7 Proton conductivity of the linear and branched comb-shaped polymer
membranes

Fig. 8 Proton conductivity of SPAEKS-main and SPAES-side

Fig. 9 Proton conductivity of the linear and branched comb-shaped polymer
membranes and Nafion 117 at 80 °C as a function of relative humidity

Fig. 10 AFM phase images of the linear and branched comb-shaped polymer

Fig. 11 The Arrhenius-type temperature-dependent proton-conductivity (σ) behavior
of the linear and branched comb-shaped polymer membranes

Fig. 12 Oxidation stability of SPAEKS-main and SPAES-side

Table 1. Properties of linear and branched comb-shaped polymers

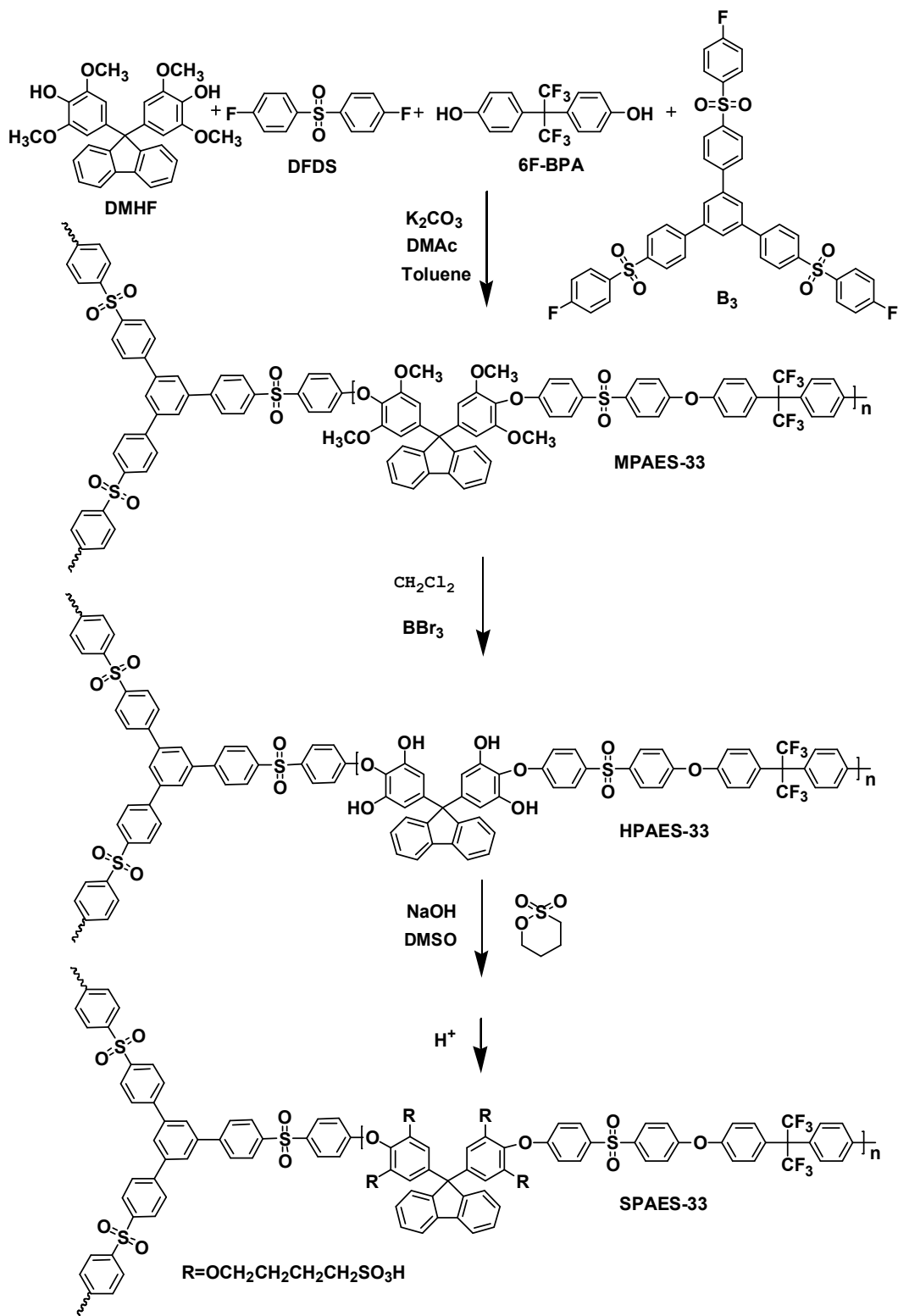
	B₃	Yield	Mn^a	Mw^a	T_{d5%}	IEC^b	IEC^c
	(%)	(%)	(×10 ⁴)	(×10 ⁴)	(°C)	(meqg ⁻¹)	(meqg ⁻¹)
SPAES-0-33	0	91	3.3	5.5	250	1.75	1.71
SPAES-4-33	4	90	66.8	77.3	252	1.71	1.70
SPAES-6-33	6	94	64.0	74.9	257	1.69	1.68
SPAES-8-33	8	89	62.3	72.7	270	1.68	1.66

^a Measured at 30 °C in THF, ^b Theoretical IEC, ^c Experimental IEC.

Table 2. Properties of linear and branched comb-shaped membranes

	Water uptake (wt%)^a	Proton conductivity (10⁻²S cm⁻¹)^b	Oxidation stability (min)	λ	Density^c (g cm⁻³)	Tensile strength (meq g⁻¹)
SPAES-0-33	34.3	23.45	220	11.2	1.57	30.15
SPAES-4-33	45.8	25.17	345	15.0	1.52	28.79
SPAES-6-33	54.8	27.29	420	18.1	1.34	24.35
SPAES-8-33	68.7	33.11	445	23.0	1.20	20.51
Nafion 117	19 ^d	10.08	>400	NR ^e	1.98 ^d	25.7 ^d

^a Measured at 80 °C, ^b measured at 80 °C and 100% relative humidity for membrane samples, ^c Based on the dry state, ^d Data taken from Ref, ^e Not reported.



Scheme 1. Synthesis of highly branched polymers MPAES-33, HPAES-33,

SPAES-33

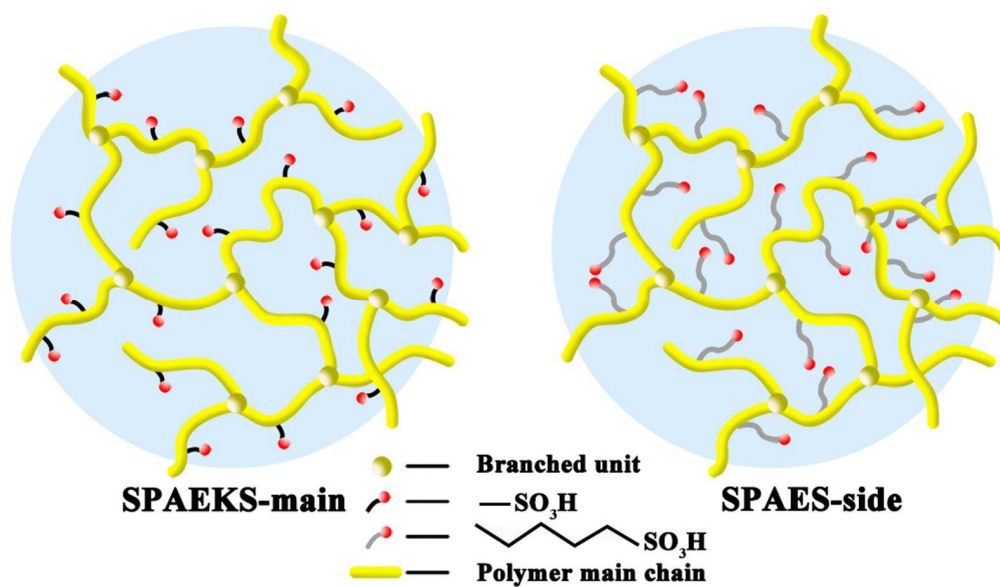


Fig. 1 Diagrams of the linear and branched comb-shaped polymers

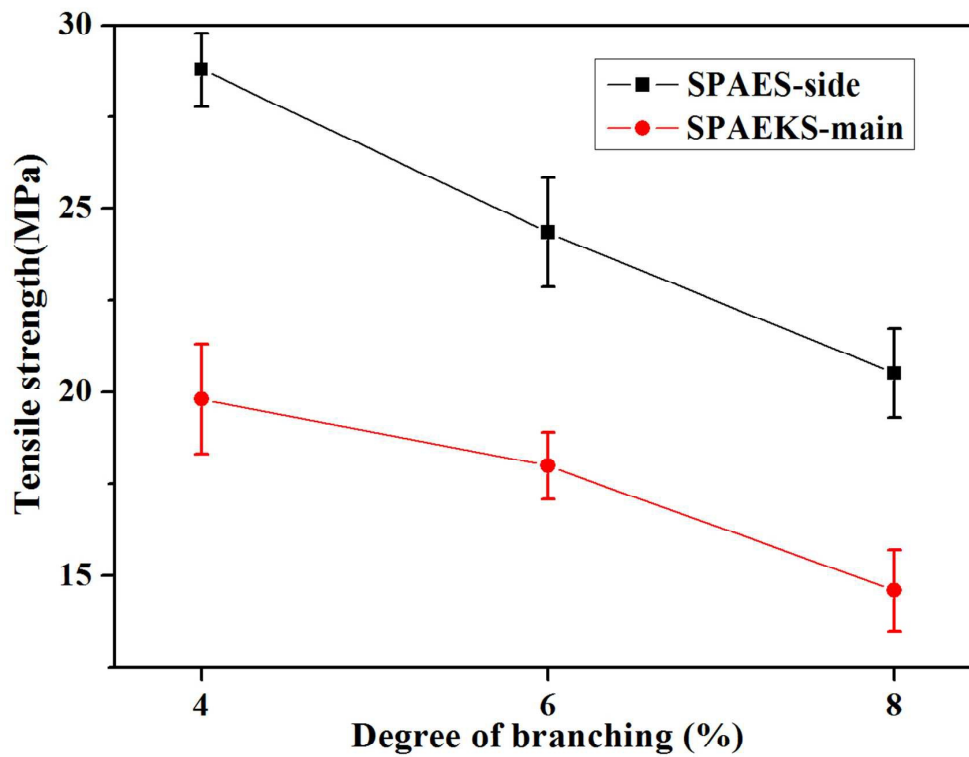


Fig. 2 Tensile strength of SPAEKS-main and SPAES-side

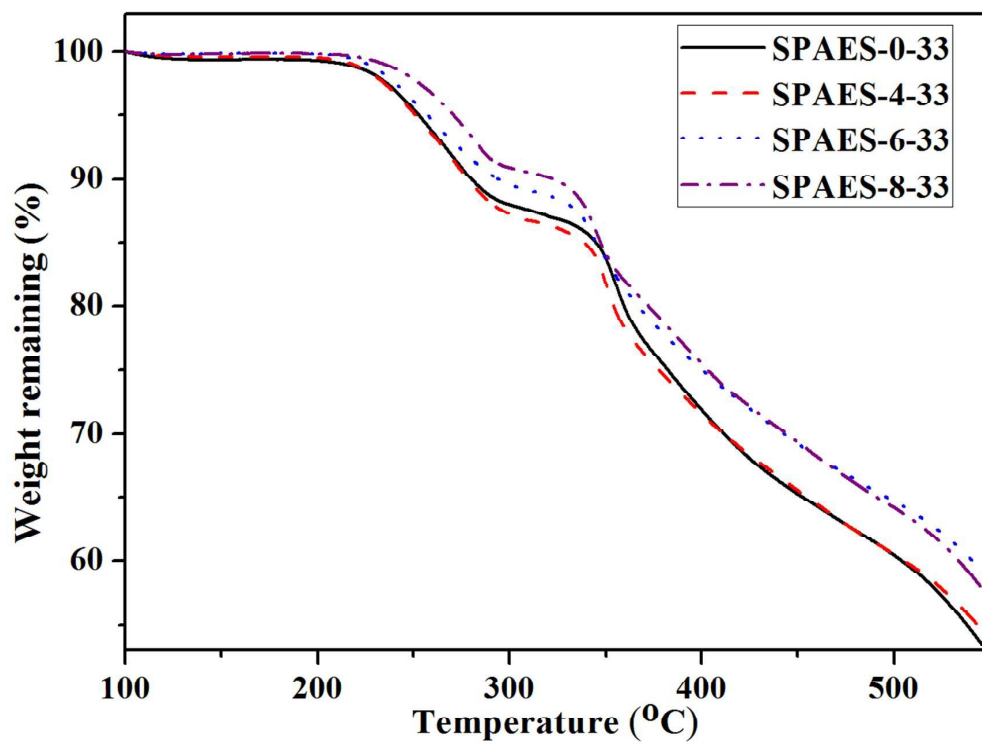


Fig. 3 TGA curves of the linear and branched comb-shaped polymers

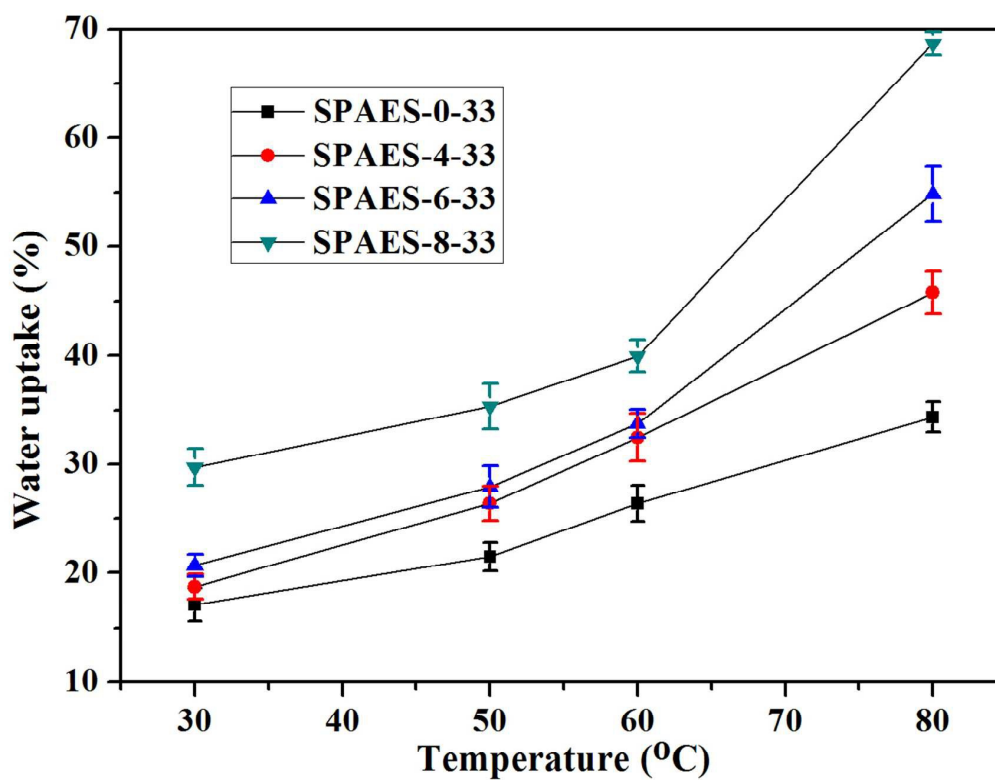


Fig. 4 Water uptake of the linear and branched comb-shaped polymer membranes

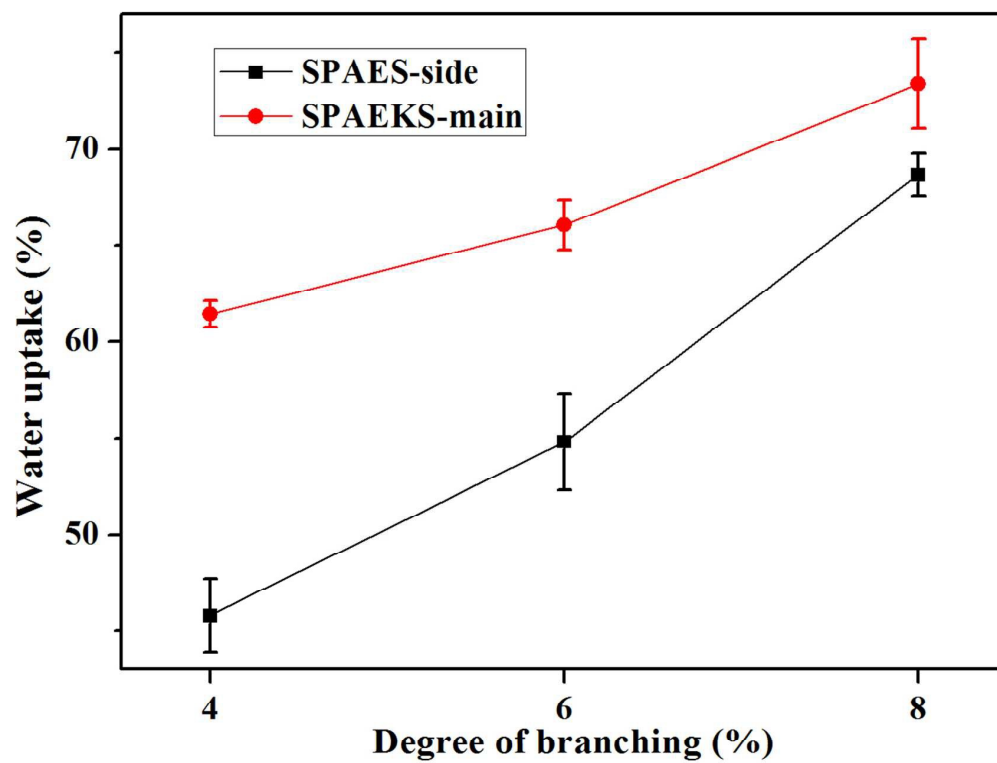


Fig. 5 Water uptake of SPAEKS-main and SPAES-side

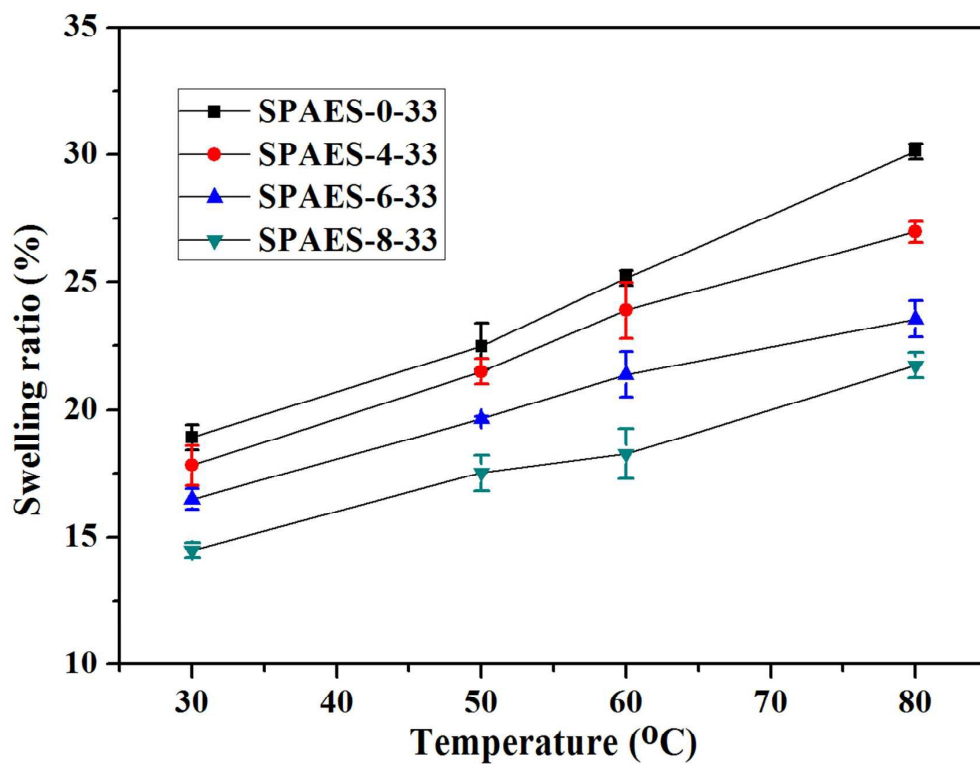


Fig. 6 Swelling rate of the linear and branched comb-shaped polymer membranes

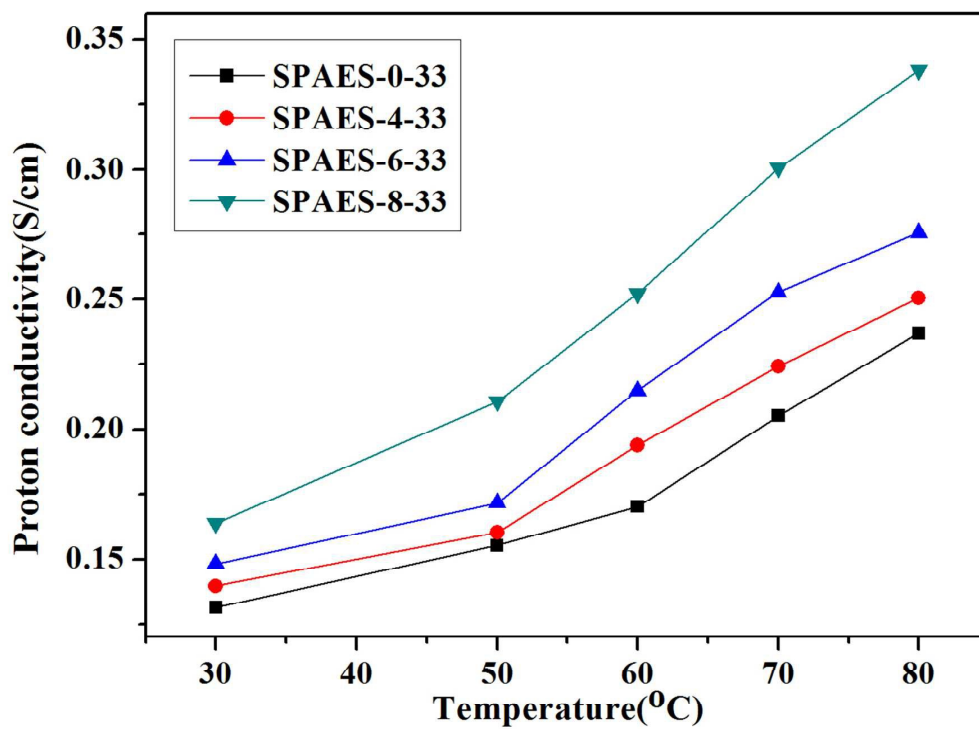


Fig. 7 Proton conductivity of the linear and branched comb-shaped polymer membranes

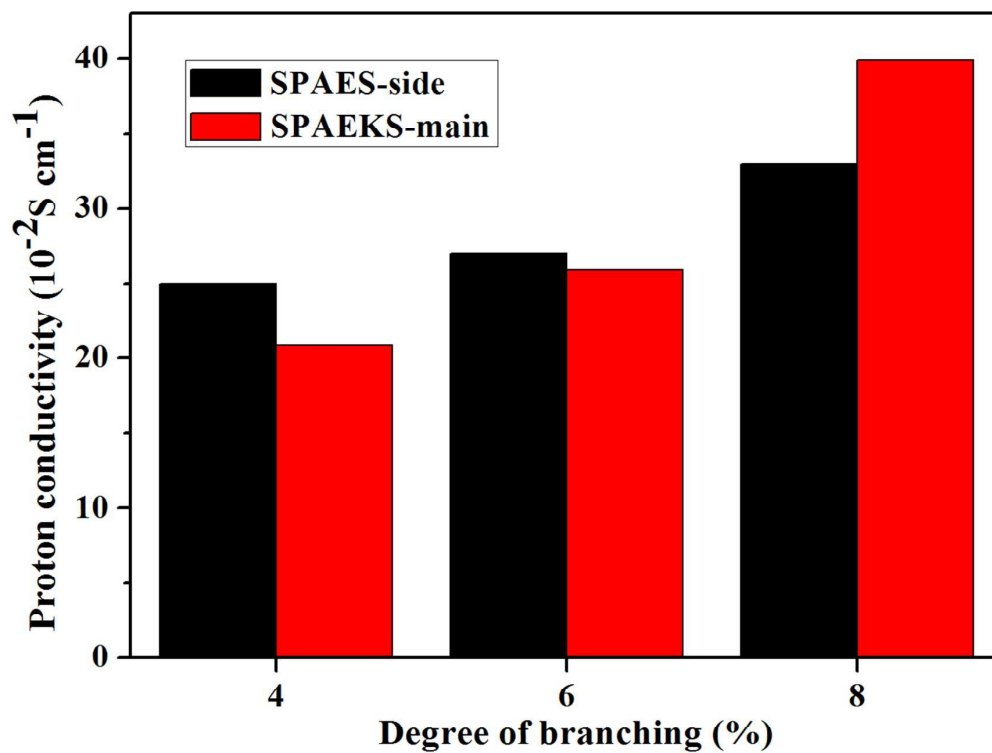


Fig. 8 Proton conductivity of SPAEKS-main and SPAES-side

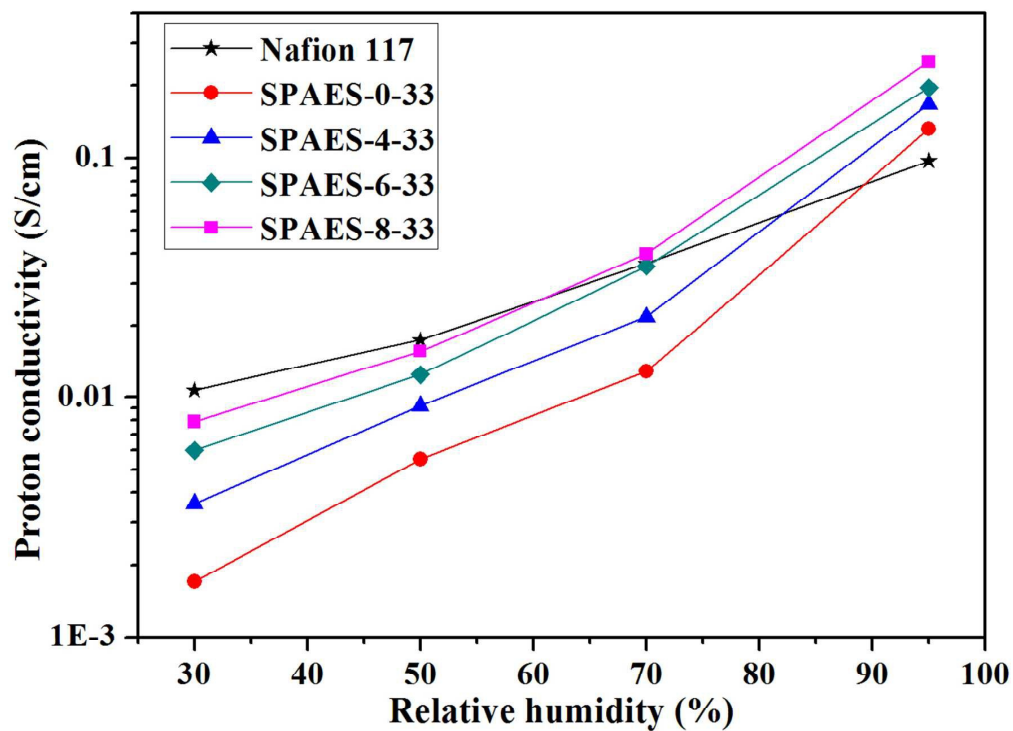


Fig. 9 Proton conductivity of the linear and branched comb-shaped polymer membranes and Nafion 117 at 80 °C as a function of relative humidity

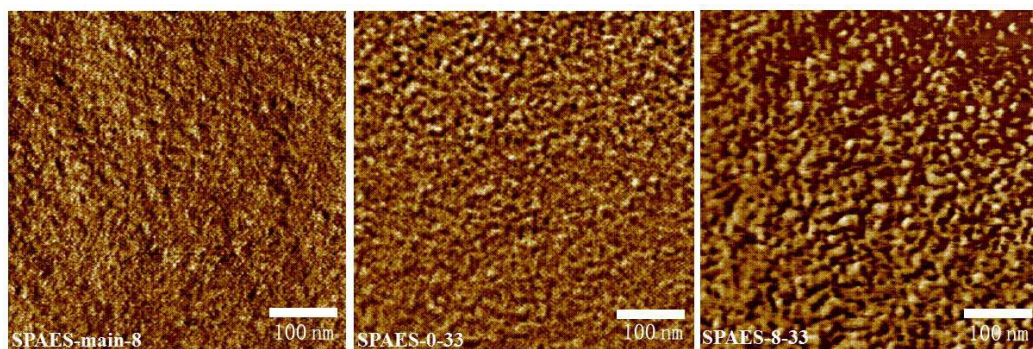


Fig. 10 AFM phase images of the linear and branched comb-shaped polymer membranes

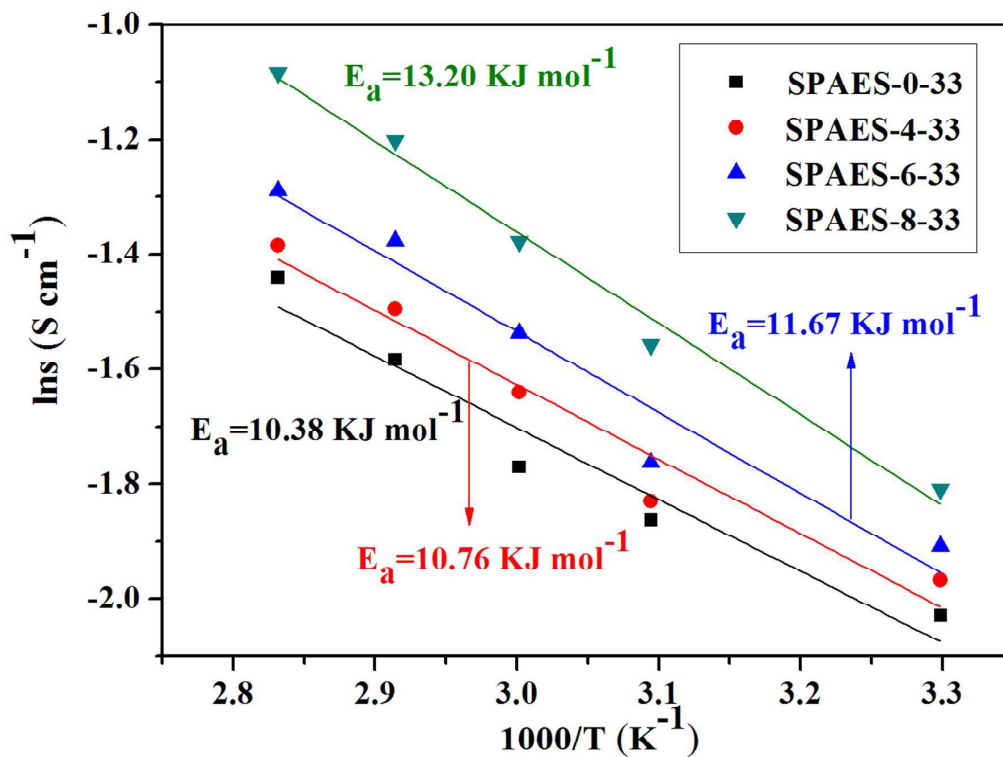


Fig. 11 The Arrhenius-type temperature-dependent proton-conductivity (σ) behavior of the linear and branched comb-shaped polymer membranes

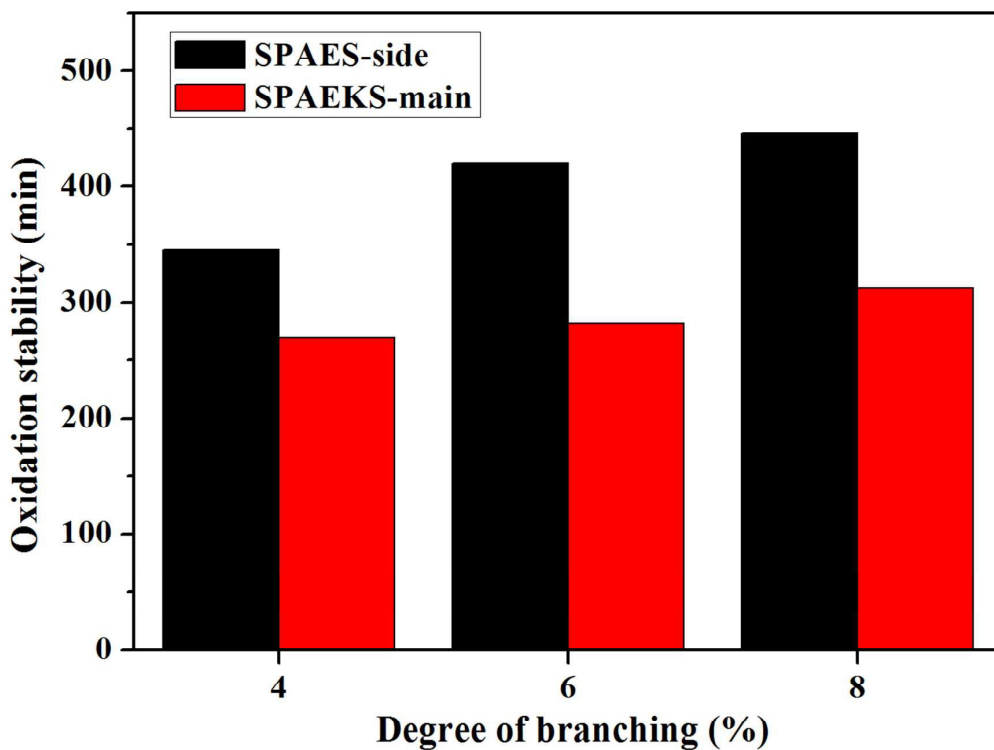


Fig. 12 Oxidation stability of SPAEKS-main and SPAES-side